11

Pediatric Cranial Ultrasound: Techniques, Variants and Pitfalls

Kristin Fickenscher[1,2], Zachary Bailey[3], Megan Saettele[1,4], Amy Dahl[1,2] and Lisa Lowe[1,2]
[1]*Department of Radiology, University of Missouri-Kansas City, Kansas City, MO,*
[2]*Department of Radiology, Children's Mercy Hospital and Clinics, Kansas City, MO,*
[3]*Kansas City University of Medicine and Biosciences, Kansas City, MO,*
[4]*Department of Radiology, Saint Luke's Hospital, Kansas City, MO,*
USA

1. Introduction

Recent advances in sonographic technology have made ultrasound an increasingly accurate and adequate means to detect cranial morphology and intracranial pathology in infants. When modern equipment is combined with thorough imaging technique, ultrasound delivers similar results to MRI in terms of sensitivity and ability to direct initial management (Daneman et. al, 2006; Epelman et. al., 2010). Furthermore, ultrasound offers certain advantages over other imaging modalities such as MRI and CT. Cranial sonography is less expensive, spares the patient from radiation, does not require sedation, and its portability allows for bedside evaluation in gravely ill infants who cannot be transported to radiology for imaging.

The goal of this chapter is to provide an updated approach to modern cranial ultrasound in order to improve diagnostic accuracy and increase recognition of normal anatomical structures, anatomical variants, pathologic processes, and imaging pitfalls that may simulate disease. The discussion will begin with an overview of the approach and interpretation of gray-scale imaging. The chapter will continue with a review of Doppler imaging, the use of additional fontanels, and linear imaging. The chapter will conclude by reviewing pitfalls and normal variants which may simulate pathology.

2. Ultrasound techniques and interpretation

2.1 Gray-scale

The cranial ultrasound examination is performed with a linear-array transducer. Six-eight coronal plane images are taken through the anterior fontanel, beginning in the frontal lobes anterior to the frontal horns and progressing posteriorly to the occipital lobes past the trigones of the lateral ventricles. (**Figure 1**) The first coronal image acquired at the level of the frontal lobes allows the observer to examine the frontal lobes, orbital cones, and the hyperechoic falx cerebri located within the interhemispheric fissure (Slovis et. al., 1981). The second coronal image is taken through the frontal horns of the lateral ventricles, which allows multiple structures to be imaged at once. The frontal horns and cavum septum pellucidum appear as

anechoic, CSF-filled spaces. The corpus callosum is a linear, hypoechoic structure crossing the hemispheres that is contained within echogenic superior and inferior borders. Finally, the globus pallidus, putamen, caudate nucleus, and thalamus of each side can be visualized in their respective locations with their characteristic gray matter appearance (Seigel, 2002). The third image is obtained at the level of the foramen of Monro and further illustrates many of the structures mentioned above. The third ventricle can be visualized as an anechoic structure beneath the septum pellucidum. Brainstem structures such as the pons and medulla can also be seen (Seigel, 2002). Moving posteriorly, the fourth image is taken at the level of the cerebral peduncles and shows hyperechoic choroid plexus along the floor of the lateral ventricles and the roof of the third ventricle. The tentorium cerebelli and fourth ventricle are also demonstrated (Seigel, 2002). The quadrigeminal plate cistern serves as a marker for the fifth image, which enables the viewer to see both temporal horns of the lateral ventricles as well as cerebellar structures including the hemispheres and vermis. Below the vermis, the cisterna magna is visible. Occasionally, the mammillary bodies can be discerned on this image (Seigel, 2002). The sixth image is taken through the lateral ventral trigones and shows their innate hyperechoic choroid plexus (Seigel, 2002). The perventricular white matter halo is also seen and should be less echogenic than the choroid plexus (Grant et. al., 1981; Seigel, 2002). The final image is obtained through the cerebral convexities and displays the interhemispheric fissure and occipital lobes (Seigel, 2002).

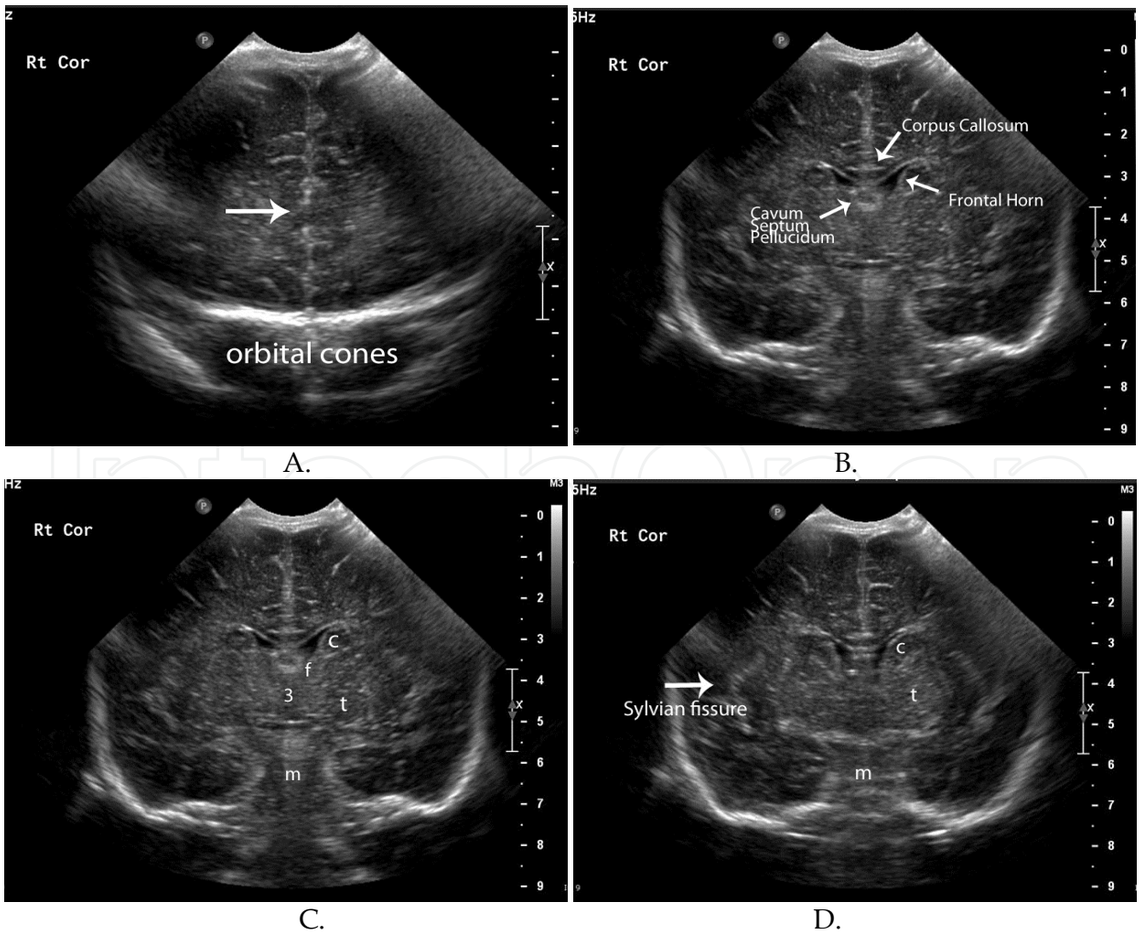

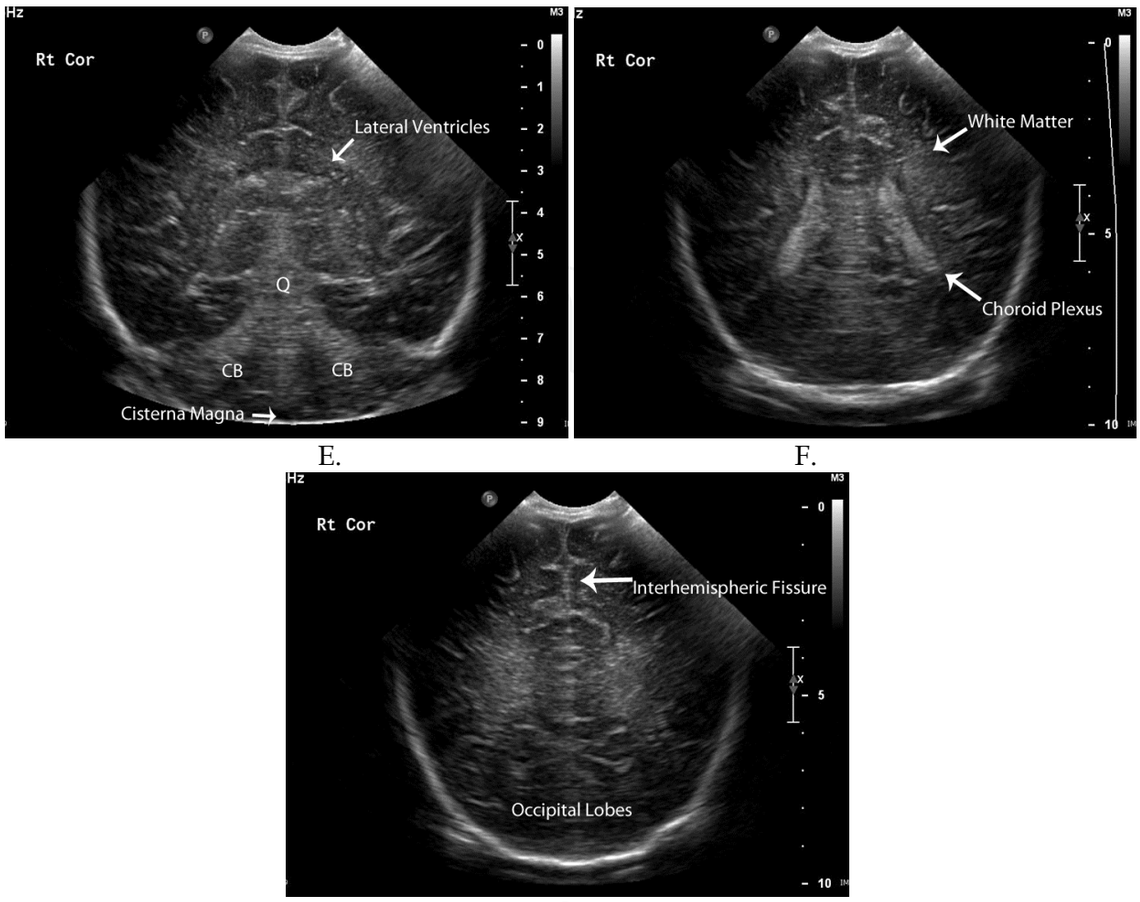

Fig. 1. (a-g). Coronal images of a normal neonatal brain. C (caudate) t (thalamus) f (Foramen of Monro) m (midbrain) 3 (third ventricle) Q (quadrigeminal plate cistern) CB (cerebellar hemispheres)

Next, the transducer is turned 90 degrees on the anterior fontanel, and five more images are acquired in the sagittal and parasagittal planes. (**Figure 2**) The first image is a midline sagittal view which includes the corpus callosum and cerebellar vermis. Additional parasagittal views are obtained laterally on either side, allowing for the inspection of the lateral horns and choroid plexus (Epelman et. al., 2010; Seigel 2002; Rumack et. al. 2005). The first midline sagittal image displays a number of important structures. The C-shaped corpus callosum appears as a hypoechoic structure bound by echogenic superior and inferior borders (Seigel, 2002). The cingulate gyrus is seen above the corpus callosum, while the septum cavum pellucidum is seen below. The third and fourth ventricles along with the cisterna magna appear anechoic at their respective positions (Seigel, 2002). The white matter containing pons and cerebellar vermis are also seen (Grant et. al., 1981 Seigel, 2002). Additional views are obtained in the parasagittal plane by cutting through the lateral ventricles. The intraventricular echogenic choroid plexus is well evaluated in this plane. The temporal lobe and caudothalamic groove, which separates the caudate nucleus from the thalamus, are also visualized. Progressing laterally, parasagittal images are obtained through the temporal horns of the lateral ventricles further demonstrating

the hyperechoic choroid plexus (Seigel, 2002). A final view can be made on either side through the lateral thalamus.

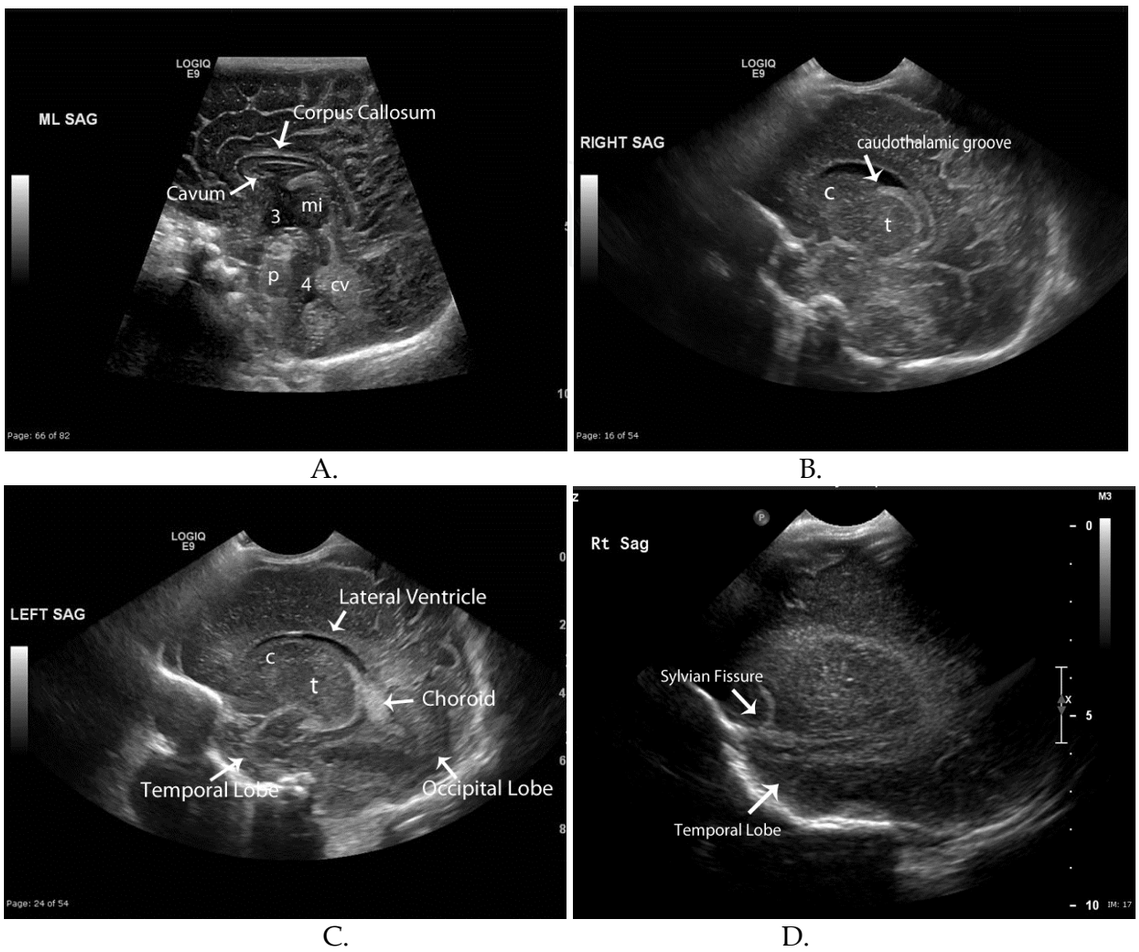

Fig. 2. (a-d). Sagittal images of a normal neonatal brain. 3 (third ventricle) mi (mass intermedia) p (belly of the pons) 4 (fourth ventricle) cv (cerebellar vermis) c (caudate nucleus) t (thalamus)

Interpretation of cranial gray-scale imaging relies not only on neuro-anatomical knowledge but also on recognition of the normal echogenic patterns of cranial structures. The following concepts are important to keep in mind when examining cranial sonographic images. Gray matter is normally hypoechoic while white matter is hyperechoic. Therefore, an anomaly is indicated when the appearance of the two is switched (North & Lowe, 2009). Secondly, though the normal brain is always symmetric, symmetry is not always normal. A prime example is seen in bilaterally symmetric hyperechoic thalami which may signal thalamic edema, ischemia, or infarct (Huang & Castillo, 2008; North & Lowe, 2009). Thirdly, it is important to visualize the pia mater, cortical gray matter, and white matter to detect focal hemorrhages and infarcts (Grant et. al. 1981). From superficial to deep, a hyperechoic, hypoechoic, hyperechoic pattern should be seen in these layers, respectively (**Figure 3**) (Slovis & Kuhns, 1981). Finally, periventricular white matter should look homogenous with

an echogenicity less than or equal to the neighboring choroid plexus (North & Lowe, 2009; Seigel, 2002). A change from this appearance including asymmetry, heterogeneity, or hyperechogenicity greater than that of adjacent choroid could be indicative of periventricular leukomalacia (**Figure 4**).

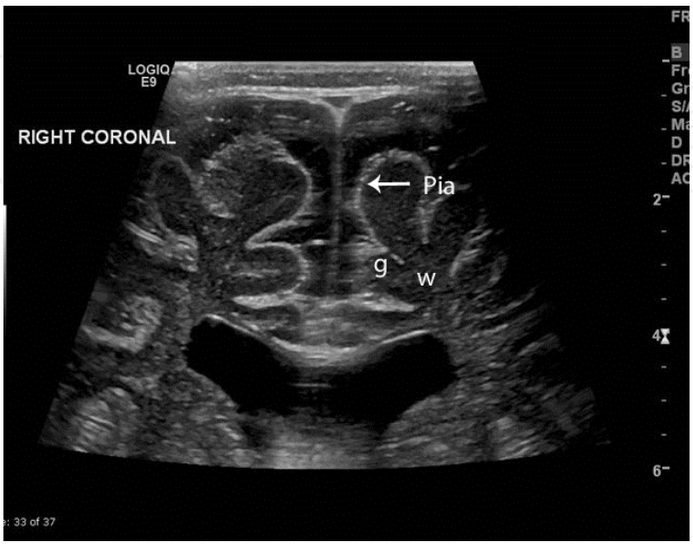

Fig. 3. High resolution linear image of the cerebral cortex. Note the hyperechoic pia matter, hypoechoic gray matter, and hyperechoic white matter. This image displays normal gray-white matter differentiation in a term neonate.

2.2 Doppler imaging

The next step in pediatric cranial sonography is Doppler screening of the vasculature (North & Lowe, 2009). First, the Circle of Willis is investigated with color Doppler imaging using either the anterior or temporal fontanels. Spectral tracings of the internal cerebral arteries are obtained and used to calculate the peak systolic velocity (PSV), end diastolic velocity (EDV), and resistive index (RI). Color Doppler images are then performed in the sagittal plane to evaluate the sagittal sinus and vein of Galen. Power Doppler imaging can be utilized to detect signs of ischemia which may present as areas of hyper- or hypovascularity (Epelman et. al., 2010).

Doppler imaging, whether color, spectral, or power, can be achieved in either the anterior or temporal fontanels according to ease or vessels to be examined (**Figure 5a &b**) (Lowe & Bulas, 2005). While either fontanel enables the inspection of the circle of Willis, use of the anterior fontanel better displays the internal cerebral arteries (**Figure 5c**) (Rumack et. al. 2005; Seigel, 2002). Color Doppler imaging is used to screen the vasculature for patency and resistance to flow. Arteries are usually evaluated in the coronal plane, while venous structures are best imaged in sagittal. Indices, including the resistive index (RI), systolic, and diastolic velocities, typically of the middle or internal cerebral arteries are obtained from spectral tracings. The RI is calculated from the peak systolic velocity and end diastolic velocity by the following formula:

$$RI = (PSV-EDV)/PSV$$

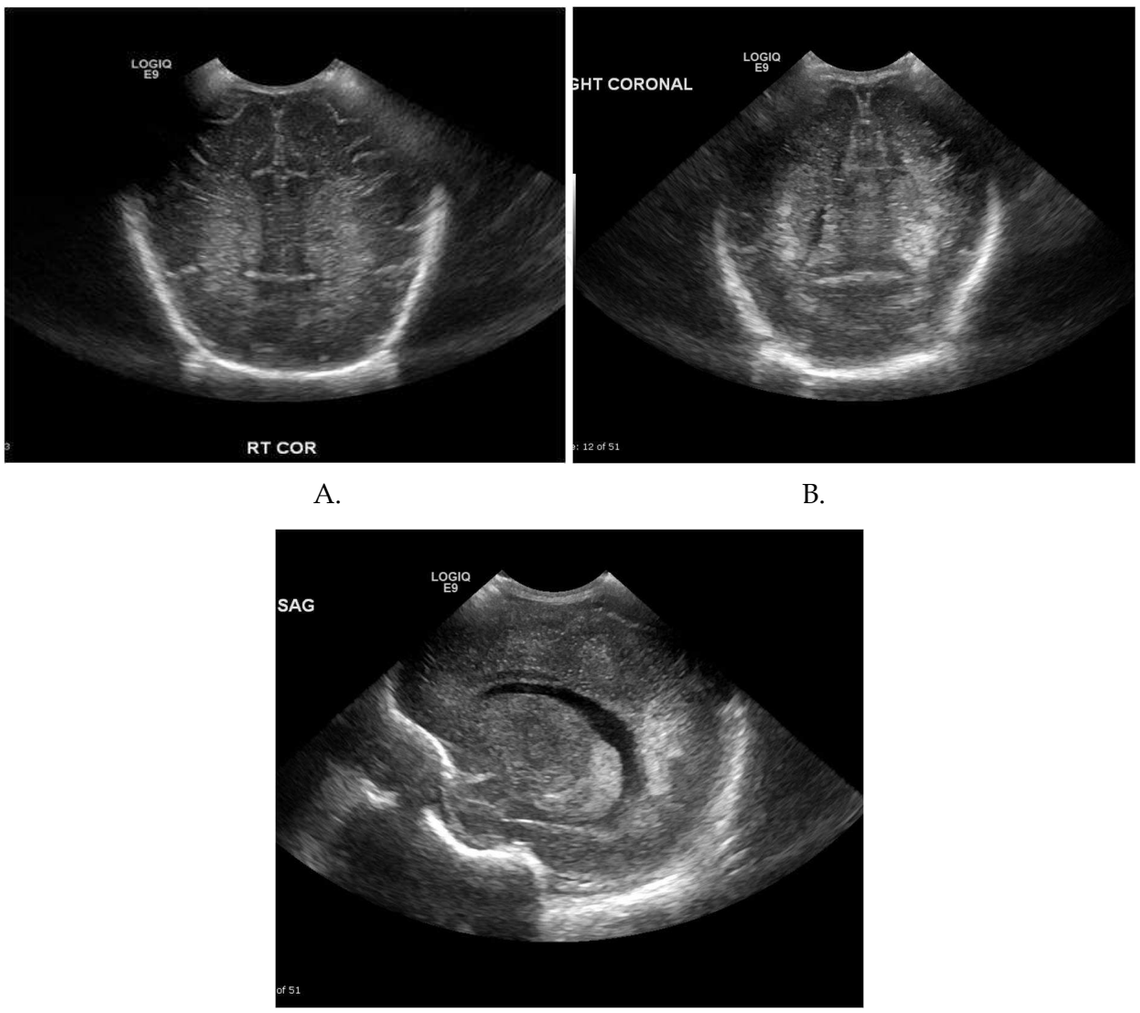

A. B.

C.

Fig. 4. (a) Normal echogenicity in the periventricular white matter is symmetric and homogenous. It is less echogenic than the neighboring choroid. (b and c) Periventricular leukomalacia is asymmetric, heterogeneous, and more echogenic than the adjacent choroid plexus.

The RI may be impacted by flow velocity, blood volume, congenital cardiac anomalies, and peripheral vascular resistance (Bulas & Vezina, 1999; Soetaert et. al., 2009). The RI tends to decline with age as diastolic flow increases with the progression from fetal to newborn circulation. Premature infants exhibit a normal RI of .62-.92 that typically drops to .43-.58 by the time the child is older than 2 years (Allison et. al., 2000; Lowe & Bulas, 2005). Therefore, a value ranging from .6-.9 is used to estimate a normal RI in premature and full-term infants. Lower values may indicate acute hypoxia or ischemia, which may trigger increased diastolic flow through cerebral vasodilation. Higher values may suggest cerebral swelling where intracranial pressures rise higher than systemic pressures leading to decreased diastolic flow (North & Lowe, 2009).

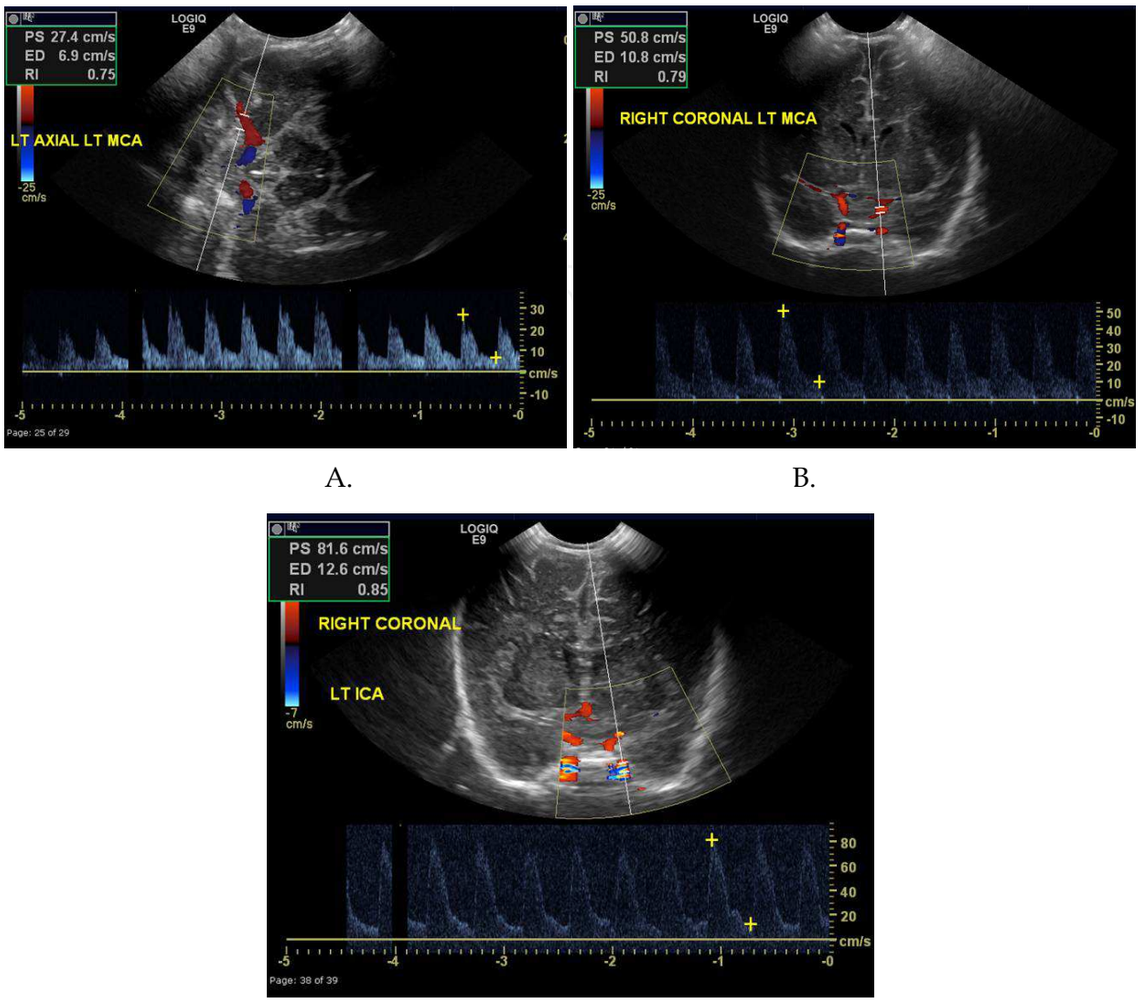

A. B.

C.

Fig. 5. (a) Axial and (b) coronal Doppler images and spectral waveforms of the normal Circle of Willis. Axial images were obtained through the temporal fontanel. Coronal images were obtained through the anterior fontanel. (c) Coronal Doppler images and spectral waveforms of a normal ICA obtained through the anterior fontanel.

As mentioned above, the RI is not always reliable. This is especially true in children with extra cardiac shunts or congenital cardiac malformations with left to right intracardiac shunt, particularly a patent ductus arteriosis (Lipman et. al., 1982). In addition, vessel velocity fluctuations are common leading to the need to acquire multiple measurements.

2.3 Additional fontanels and linear imaging

A state of the art approach to head sonography requires utilization of additional fontanels and high-resolution linear imaging. The mastoid fontanels enable inspection of the cerebellar hemispheres and aid in detection of posterior fossa hemorrhages and congenital anomalies (**Figure 6**) (Di Salvo, 2001). Mastoid fontanels are also used to evaluate the size and appearance of the fourth ventricle and cisterna magna. Due to improved posterior fossa hemorrhage discovery, these views are now part of the standard of care for hindbrain

imaging (Seigel, 2002). The transverse sinuses can be examined through posterior fontanels or foramen magnum. Color Doppler can aid in evaluating vascular flow and patency (Brennan et. al., 2005; Epelman et. al, 2010; Lowe & Bulas, 2005, Sudakoff et. al., 1993).
Linear imaging should be used to assess the subarachnoid space and superficial cortex via the anterior fontanel (**Figure 7**) (Epelman et. al., 2010). Supplementary fontanels may be explored to gain accessory views.

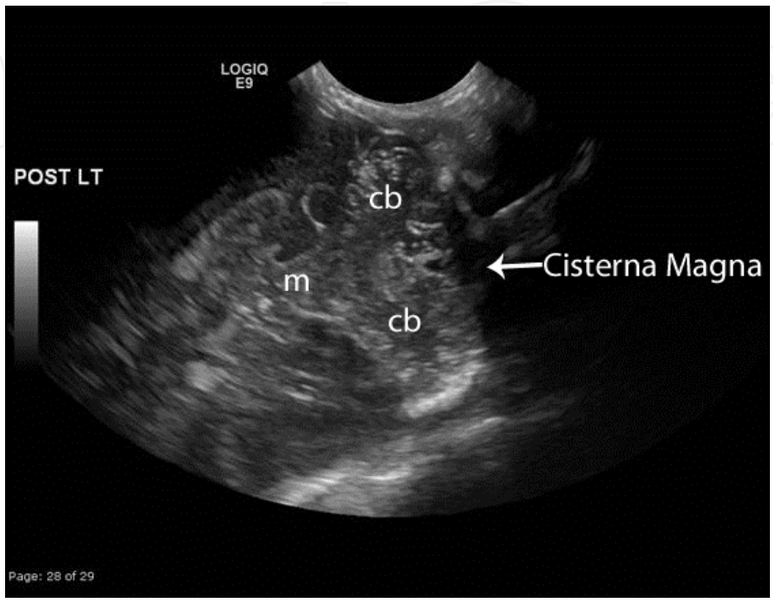

Fig. 6. Normal posterior fossa image obtained using the mastoid fontanel.
cb (cerebellar hemispheres) m (midbrain)

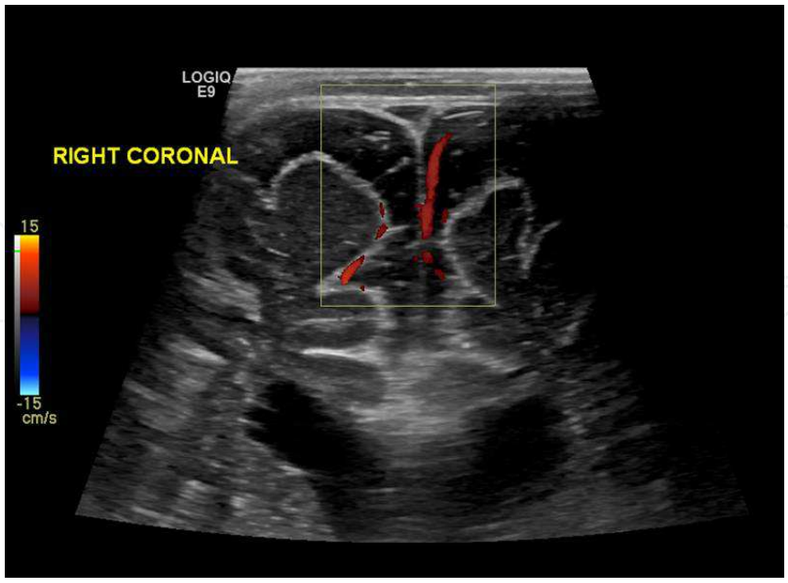

Fig. 7. High resolution linear image demonstrating prominent extra axial CSF spaces. Doppler interrogation demonstrates a vessel crossing the space, confirming subarachnoid fluid rather than subdural.

3. Pitfalls and normal variants

3.1 Immature sulcation in premature infants

The infant brain becomes increasingly sulcated during development. Cerebral cortices in neonates born prior to the 24th week gestational age contain only Sylvian fissures in an otherwise smooth cerebral cortex making lissencephaly in this age group an avoidable diagnosis (**Figure 8**). At 24 weeks gestational age, the parietooccipital fissure is seen. This is followed by the appearance of the cingulate sulci at 28 weeks gestational age with additional branching occurring into full term (North & Lowe, 2009; Rumack et. al., 2005).

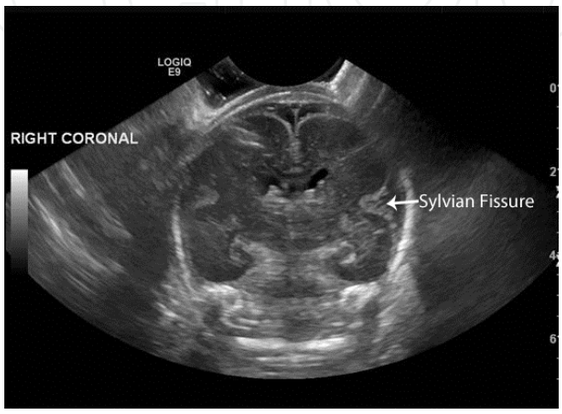

Fig. 8. Coronal image of a 24 week gestation preterm infant. Note the lack of cerebral sulci. Only the Sylvian Fissures are clearly visible.

3.2 Persistent fetal fluid-filled spaces

Healthy infants commonly exhibit persistent fetal fluid-filled spaces. Typical findings consist of cavum septum pellucidum (CSP), cavum vergae, and cavum veli interpositi. Usually, these spaces start to close around the 6th month of gestational age, and most (85%) are completely closed by 3-6 months of chronological age, although some may remain present into adulthood (Epelman, 2006; Faruggia & Babcock, 1981; Needleman et. al., 2007; Osborn, 1991). The CSP is a midline fluid-filled space located anteriorly and between the frontal horns of the lateral ventricles (**Figure 9**). It is formed from failed septal laminae fusion (Epelman, 2006). If the space extends posterior to the fornices, it is termed cavum vergae. (Bronshtein & Weiner, 1992; Epelman et. al., 2006). A cavum veli interpositi is located even further posteriorly as a separate fluid-filled space found in the pineal region. Due to the location of the cavum veli interpositi. It must be distinguished from other commonly occurring manifestations in this region, specifically, congenital pineal cysts and vein of Galen malformations (Chen et. al., 1998; Epelman et. al., 2006).

3.3 Mega cisterna magna

A mega cisterna magna is defined as a cisterna magna that measures greater than 8mm in either sagittal or axial planes. It is present in approximately 1% of infant brains and is a benign finding of no clinical significance. It is, therefore, key not to mistake a mega cisterna magna for other malformations that can occur in the posterior fossa (Bernard et. al., 2001; Epelman et.al., 2006; Nelson et. al., 2004). Unlike arachnoid cysts, a mega cisterna magna will not exhibit mass effect on adjacent structures. It can also be differentiated from Dandy-

Walker malformations by visualization of the cerebellar vermis (Epelman et.al., 2006; Nelson et. al., 2004).

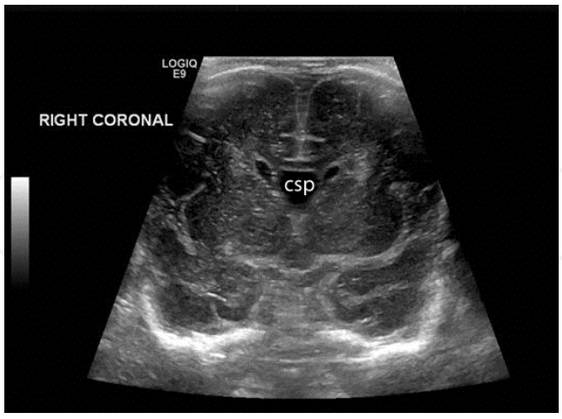

Fig. 9. Coronal image of a term neonate demonstrating a midline fluid-filled space between the frontal horns of the lateral ventricles consistent with a cavum septum pellucidum (csp).

3.4 Asymmetric ventricular size

20-40% of infants may exhibit asymmetrical ventricular size (Middleton et. al., 2009; Seigel, 2002; Winchester et. al., 1986). This can appear as a discrepancy between the frontal and occipital horn size termed colpocephaly or as variations in sizes of the left and right ventricles. The former may co-occur with agenesis of the corpus callosum or Chiari II malformations. (Achiron et. al., 1997; Horbar et. al., 1983; Seigel, 2002). The latter is a common finding in which the less dependent ventricle is the largest. The left ventricle is most commonly the bigger of the two with sizes varying depending on patient position (Enriquez et. al., 2003; Koeda et. al., 1988; Seigel, 2002).

3.5 Choroid plexus variants

The choroid plexus is located at the roof of the third ventricle and travels through the foramen of Monro into the lateral ventricles (North & Lowe, 2009; Seigel, 2002). It does not extend into the frontal or occipital horns, so hyperechoic material in these areas should suggest pathology. Choroid appearing substance anterior to the caudothalamic groove is likely a germinal matrix hemorrhage, while interventricular hemorrhage may be indicated by hyperechoic material in the dependent portions of the occipital horns (Grant et. al., 1983; Seigel, 2002). Choroid plexus morphology, however, is variable and should not be confused with hemorrhage. This is especially true in the glomus of the lateral ventricles and ventricular atria where lobular and bulbous choroid is commonly seen (**Figure 10**). The occipital horns may also display bulbous and drumstick-shaped choroid variations, particularly in conjunction with Chiari II malformations (Di Salvo, 2001; Seigel, 2002).

In addition, choroid cysts are commonly identified (**Figure 11**). When seen in isolation and measuring less than 1cm, they are considered a benign finding (DeRoo et. al., 1988; Epelman et. al., 2006; Ostlere et. al., 1990; van Baalen & Versmold, 2004). When choroid cysts are found to be multiple, bilateral, or greater than 1 cm in size, this may suggest a chromosomal abnormality (Gupta et. al., 1995; Seigel, 2002).

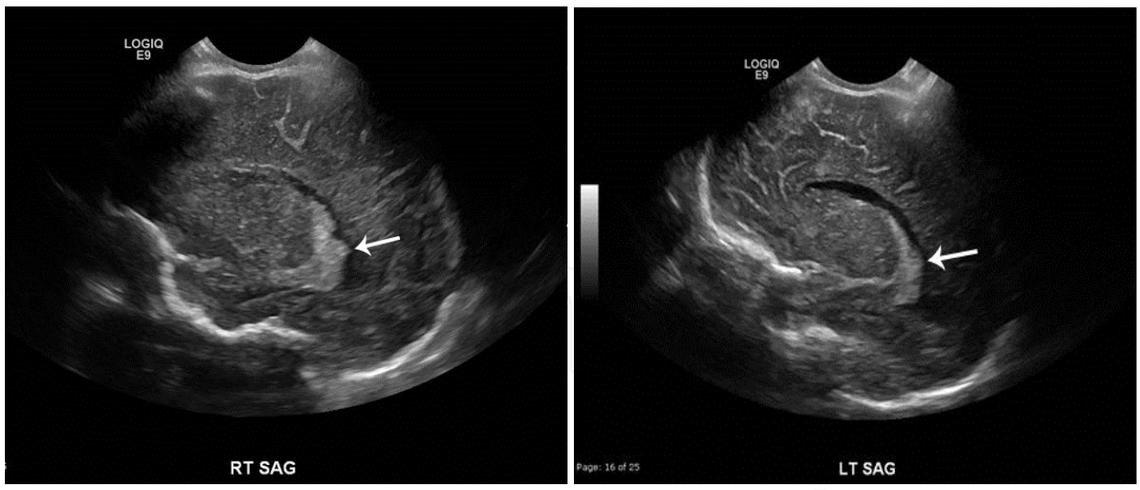

A. B.

Fig. 10. Sagittal images of the (a) right and (b) left lateral ventricles demonstrating asymmetry in the choroid plexus (arrows) with the right being larger and more lobulated than the left. Both are normal.

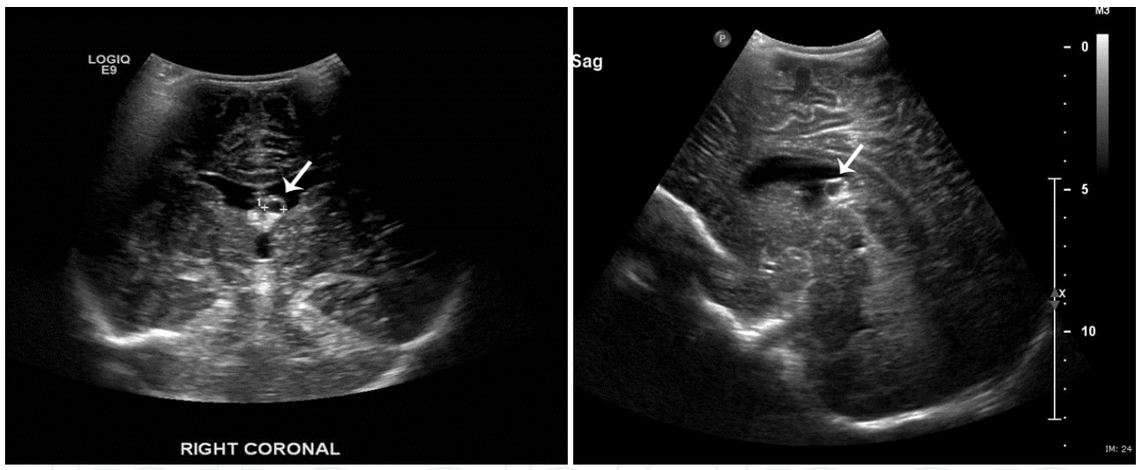

A. B.

Fig. 11. Coronal (a) and Sagittal (b) images demonstrate and anechoic, cystic structure (arrows) arising from the anterior choroid consistent with a choroid plexus cyst.

3.6 Periventricular cystic lesions

Connatal cysts, subependymal cysts, germinolytic cysts, and white matter cysts can all appear in the periventricular area (Epelman et. al., 2006; North & Lowe, 2009). Connatal cysts are always found in immediate proximity with the frontal horns where they are found in multiples and exhibit a string of pearls appearance (**Figure 12**). They are a normal variant believed to be caused by deficient coaptation of the ventricles (Chang et. al., 2006; Enriquez et. al., 2003; Epelman et. al, 2006; Pal et. al., 2001; Rosenfeld et. al., 1997). These cysts are often discovered shortly after birth and usually undergo spontaneous regression (Chang et. al., 2006; Rosenfeld et. al., 1997). Subependymal cysts and germinolytic cysts both occur at

the caudothalamic groove. Subependymal cysts are the sequlae of germinal matrix hemorrhages and geminolytic cysts are commonly seen in metabolic disorders. Despite the differing pathophysiology, the imaging characteristics are identical and the two cysts cannot be distinguished from one another. (Epelman et. al., 2006; Herini et. al., 2003). Lastly, hypoxia and ischemic injury in preterm infants can lead to white matter cysts located near the lateral ventricles in cases of cystic periventricular leukomalacia (**Figure 13**) (Epelman et. al., 2006; North & Lowe, 2009).

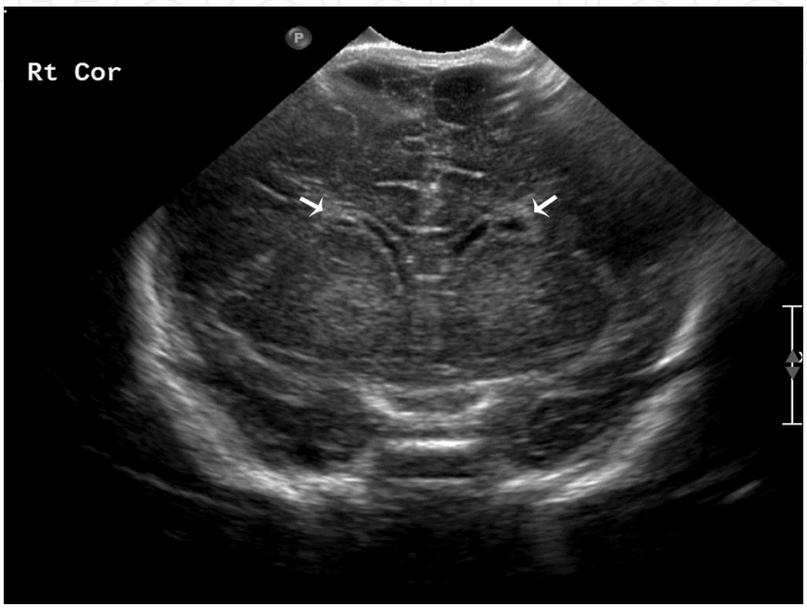

Fig. 12. Cystic lesions in the bilateral frontal periventricular white matter (arrows) consistent with connatal cysts. Connatal cysts are considered to be a normal variant.

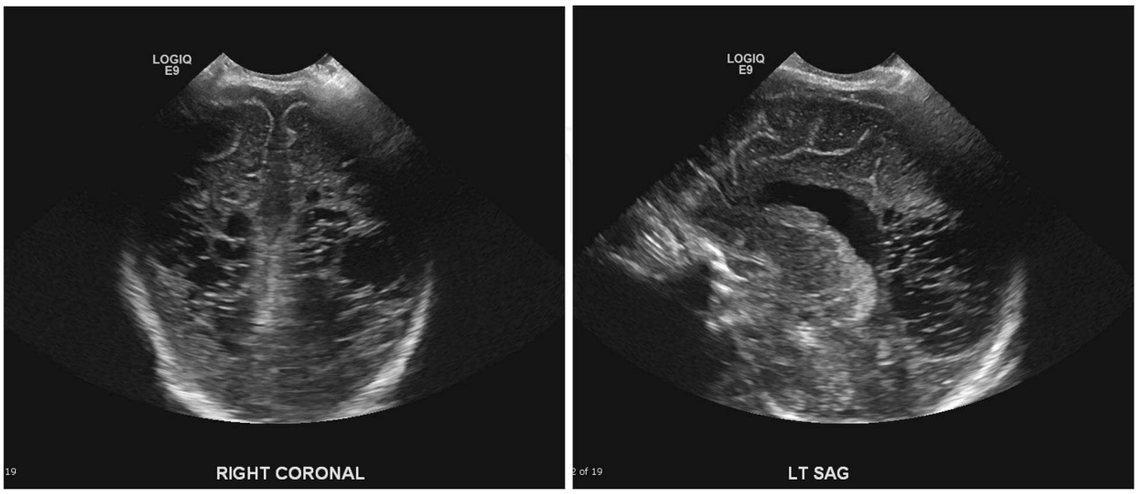

A. B.

Fig. 13. (a) Coronal and (b) Sagittal images demonstrating multiple cystic lesions in the posterior periventricular white matter consistent with cystic periventricular leukomalacia.

3.7 Periventricular halos

Periventricular halos are hyperechoic white matter pseudolesions found adjacent to ventricles (**Figure 14**). They are discovered more often in preterm than term infants and are caused by anisotropic effect. These artifacts tend to disappear on tangential imaging and should have less echogenicity than neighboring choroid plexus (Enriquez et. al., 2003; Seigel, 2002). Linear imaging may serve a complimentary role in evaluation, helping distinguish between normal and abnormal processes. Pathological findings such as periventricular hemorrhage, leukmalacia, or other abnormalities, are seen in two planes (DiPietro et. al., 1986; Schafer et. al., 2009).

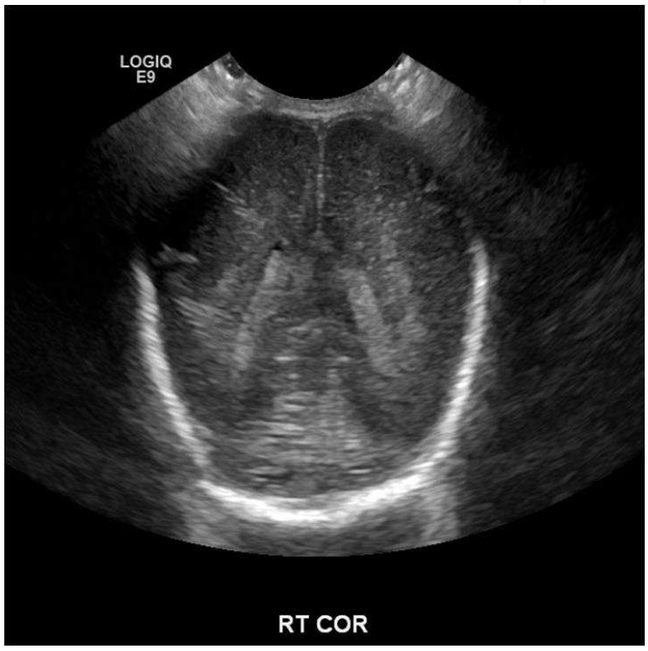

Fig. 14. Coronal image in a premature infant (note the lack of sulci) demonstrating hyperechoic psedudolesions in the periventricular white matter consistent with normal "periventricular halo". This should not be confused with the more echogenic, less homogeneous findings of periventricular luekomalacia.

3.8 Lenticulostriate vasculopathy

Lenticulostriate vasculopathy appears as linear, branching or punctate increased echogenicity within the thalami (**Figure 15**). It can be unilateral or bilateral (Cabanas et. al., 1994; Coley et. al., 2000; Makhoul et. al., 2003). It is associated with congenital infections (TORCH infections), metabolic syndromes (peroxisomal biogenesis disorders), severe congenital heart disease, and chromosomal anomalies (Patau's syndrome) which are all believed to cause lenticulostriate artery wall thickening (Cabanas et. al. 1994; Leijser et. al., 2007; Makhoul et. al., 2003; Te Pas et. al., 2005; Teele et. al., 1988). Sometimes, however, no specific cause can be ascertained making lenticulostriate vasculopathy a non-specific finding on sonography(Cabanas et. al., 1994; Coley et. al., 2000; Makhoul et. al., 2003).

Fig. 15. Sagittal image of the right lateral ventricle and thalamus demonstrating echogenic linear and branching vessels in the thalamus consistent with lenticulostriate vasculopthy.

4. Conclusion

Technical advances in ultrasound examination have made this a highly sensitive means to detect and guide treatment for pediatric cranial pathologies. When performing a head ultrasound, it is important to use modern modalities to full advantage. Doppler and linear sonography as well as the use of additional fontanels play a key role in the evaluation of the pediatric brain. Further knowledge of normal anatomy, normal variants, and imaging pitfalls increases diagnostic accuracy and helps to limit misdiagnoses.

5. References

Achiron R, Yagel S, Rotstein Z, Inbar O, Mashiach S, Lipitz S. Cerebral lateral ventricular asymmetry: is this a normal ultrasonographic finding in the fetal brain? *Obstet Gynecol* 1997; 89:233–237

Allison JW, Faddis LA, Kinder DL, Roberson PK, Glasier CM, Seibert JJ. Intracranial resistive index (RI) values in normal term infants during the first day of life. *Pediatr Radiol* 2000; 30:618–620

Bernard JP, Moscoso G, Renier D, Ville Y. Cystic malformations of the posterior fossa. *Prenat Diagn* 2001; 21:1064-1069

Brennan KC, Lowe LH, Yeaney GA. Pediatric central nervous system posttransplant lymphoproliferative disorder. *AJNR* 2005; 26:1695–1697

Bronshtein M, Weiner Z. Prenatal diagnosis of dilated cava septi pellucidi et vergae: associated anomalies, differential diagnosis, and pregnancy outcome. *Obstet Gynecol* 1992; 80:838–842

Bulas DI, Vezina GL. Preterm anoxic injury: radiologic evaluation. *Radiol Clin North Am* 1999; 37:1147–1161

Cabanas F, Pellicer A, Morales C, Garcia-Alix A, Stiris TA, Quero J. New pattern of hyperechogenicity in thalamus and basal ganglia studied by color Doppler flow imaging. *Pediatr Neurol* 1994; 10:109–116

Chang CL, Chiu NC, Ho CS, Li ST. Frontal horn cysts in normal neonates. *Brain Dev* 2006; 28: 426–430

Chen CY, Chen FH, Lee CC, Lee KW, Hsiao HS. Sonographic characteristics of the cavum velum interpositum. *AJNR* 1998; 19:1631–1635

Coley BD, Rusin JA, Boue DR. Importance of hypoxic/ischemic conditions in the development of cerebral lenticulostriate vasculopathy. *PediatrRadiol* 2000; 30:846–855

Daneman A, Epelman M, Blaser S, Jarrin JR. Imaging of the brain in full-term neonates: does sonography still play a role? *Pediatr Radiol* 2006; 36:636–646

DeRoo TR, Harris RD, Sargent SK, Denholm TA, Crow HC. Fetal choroid plexus cysts: prevalence, clinical significance, and sonographic appearance. *AJR* 1988; 151:1179–1181

DiPietro MA, Brody BA, Teele RL. Peritrigonal echogenic "blush" on cranial sonography: pathologic correlates. *AJR* 1986; 146:1067–1072

Di Salvo DN. A new view of the neonatal brain: clinical utility of supplemental neurologic US imaging windows. *RadioGraphics* 2001; 21:943–955

Enriquez G, Correa F, Lucaya J, Piqueras J, Aso C, Ortega A. Potential pitfalls in cranial sonography. *Pediatr Radiol* 2003; 33:110–117

Epelman M. The whirlpool sign. *Radiology* 2006; 240:910–911

Epelman M, Daneman A, Blaser SI, et al. Differential diagnosis of intracranial cystic lesions at head US: correlation with CT and MR imaging. *RadioGraphics* 2006; 26:173–196

Epelman M, Daneman A, Kellenberger CJ, et al. Neonatal encephalopathy: a prospective comparison of head US and MRI. *Pediatr Radiol* 2010; 40:1640–1650

Farruggia S, Babcock DS. The cavum septi pellucidi: its appearance and incidence with cranial ultrasonography in infancy. *Radiology* 1981; 139: 147–150

Grant EG, Schellinger D, Borts FT, et al. Realtime sonography of the neonatal and infant head. *AJR* 1981; 136:265–270

Grant EG, Schellinger D, Richardson JD, Coffey ML, Smirniotopoulous JG. Echogenic periventricular halo: normal sonographic finding or neonatal cerebral hemorrhage. *AJR* 1983; 140:793–796

Gupta JK, Cave M, Lilford RJ, et al. Clinical significance of fetal choroid plexus cysts. *Lancet* 1995; 346:724–729

Herini E, Tsuneishi S, Takada S, Sunarini, Nakamura H. Clinical features of infants with subependymal germinolysis and choroid plexus cysts. *Pediatr Int* 2003; 45:692–696

Horbar JD, Leahy KA, Lucey JF. Ultrasound identification of lateral ventricular asymmetry in the human neonate. *J Clin Ultrasound* 1983; 11:67–69

Huang BY, Castillo M. Hypoxic-ischemic brain injury: imaging findings from birth to adulthood. *RadioGraphics* 2008; 28:417–439; quiz, 617

Koeda T, Ando Y, Takashima S, Takeshita K, Maeda K. Changes in the lateral ventricle with the head position: ultrasonographic observation. *Neuroradiology* 1988; 30:315–318

Leijser LM, de Vries LS, Rutherford MA, et al. Cranial ultrasound in metabolic disorders presenting in the neonatal period: characteristic features and comparison with MR imaging. *AJNR* 2007; 28:1223–1231

Lipman B, Serwer GA, Brazy JE. Abnormal cerebral hemodynamics in preterm infants with patent ductus arteriosus. *Pediatrics* 1982; 69:778–781

Lowe LH, Bulas DI. Transcranial Doppler imaging in children: sickle cell screening and beyond. *Pediatr Radiol* 2005; 35:54–65

Makhoul IR, Eisenstein I, Sujov P, et al. Neonatal lenticulostriate vasculopathy: further characterisation. *Arch Dis Child Fetal Neonatal Ed* 2003; 88:F410–F414

Middleton WD, Kurtz AB, Hertzbert BS. *Ultrasound: the requisites*. St. Louis, MO: Mosby-Year Book, 2009:377

Needelman H, Schroeder B, Sweeney M, Schmidt J, Bodensteiner JB, Schaefer GB. Postterm closure of the cavum septi pellucidi and developmental outcome in premature infants. *J Child Neurol* 2007; 22:314–316

Nelson MD Jr, Maher K, Gilles FH. A different approach to cysts of the posterior fossa. *Pediatr Radiol* 2004; 34:720–732

North K, Lowe L. Modern head ultrasound: normal anatomy, variants, and pitfalls that may simulate disease. *Ultrasound Clin* 2009; 4:497–512

Osborn A. *Handbook of neuroradiology*. St. Louis, MO: Mosby-Year Book, 1991

Ostlere SJ, Irving HC, Lilford RJ. Fetal choroid plexus cysts: a report of 100 cases. *Radiology* 1990; 175:753–755

Pal BR, Preston PR, Morgan ME, Rushton DI, Durbin GM. Frontal horn thin walled cysts in preterm neonates are benign. *Arch Dis Child Fetal Neonatal Ed* 2001; 85:F187–F193

Rosenfeld DL, Schonfeld SM, Underberg-Davis S. Coarctation of the lateral ventricles: an alternative explanation for subependymal pseudocysts. *Pediatr Radiol* 1997; 27:895–897

Rumack C, Wilson S, Charboneau J. *Diagnostic ultrasound*. St. Louis, MO: Mosby, 2005

Schafer RJ, Lacadie C, Vohr B, et al. Alterations in functional connectivity for language in prematurelyborn adolescents. *Brain* 2009; 132:661–670

Seigel M, ed. *Pediatric sonography*, 3rd ed. Philadelphia, PA: Lippincott Williams & Wilkins, 2002

Slovis TL, Kuhns LR. Real-time sonography of the brain through the anterior fontanel. *AJR* 1981; 136:277–286

Soetaert AM, Lowe LH, Formen C. Pediatric cranial Doppler sonography in children: non-sickle cell applications. *Curr Probl Diagn Radiol* 2009; 38:218–227

Sudakoff GS, Montazemi M, Rifkin MD. The foramen magnum: the underutilized acoustic window to the posterior fossa. *J Ultrasound Med* 1993; 12:205–210

Te Pas AB, van Wezel-Meijler G, Bokenkamp-Gramann R, Walther FJ. Preoperative cranial ultrasound findings in infants with major congenital heart disease. *Acta Paediatr* 2005; 94:1597–1603

Teele RL, Hernanz-Schulman M, Sotrel A. Echogenic vasculature in the basal ganglia of neonates:a sonographic sign of vasculopathy. *Radiology* 1988; 169:423–427

van Baalen A, Versmold H. Choroid plexus cyst: comparison of new ultrasound technique with old histological finding. *Arch Dis Child* 2004; 89:426

Winchester P, Brill PW, Cooper R, Krauss AN, Peterson HD. Prevalence of "compressed" and asymmetric lateral ventricles in healthy full-term neonates: sonographic study. *AJR* 1986; 146

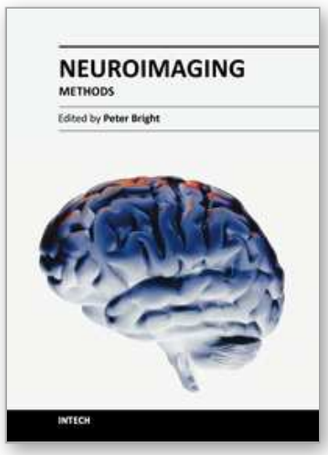

Neuroimaging - Methods

Edited by Prof. Peter Bright

ISBN 978-953-51-0097-3
Hard cover, 358 pages
Publisher InTech
Published online 17, February, 2012
Published in print edition February, 2012

Neuroimaging methodologies continue to develop at a remarkable rate, providing ever more sophisticated techniques for investigating brain structure and function. The scope of this book is not to provide a comprehensive overview of methods and applications but to provide a 'snapshot' of current approaches using well established and newly emerging techniques. Taken together, these chapters provide a broad sense of how the limits of what is achievable with neuroimaging methods are being stretched.

How to reference

In order to correctly reference this scholarly work, feel free to copy and paste the following:

Kristin Fickenscher, Zachary Bailey, Megan Saettele, Amy Dahl and Lisa Lowe (2012). Pediatric Cranial Ultrasound: Techniques, Variants and Pitfalls, Neuroimaging - Methods, Prof. Peter Bright (Ed.), ISBN: 978-953-51-0097-3, InTech, Available from: http://www.intechopen.com/books/neuroimaging-methods/pediatric-cranial-ultrasound-techniques-variants-and-pitfalls

INTECH
open science | open minds

InTech Europe
University Campus STeP Ri
Slavka Krautzeka 83/A
51000 Rijeka, Croatia
Phone: +385 (51) 770 447
Fax: +385 (51) 686 166
www.intechopen.com

InTech China
Unit 405, Office Block, Hotel Equatorial Shanghai
No.65, Yan An Road (West), Shanghai, 200040, China
中国上海市延安西路65号上海国际贵都大饭店办公楼405单元
Phone: +86-21-62489820
Fax: +86-21-62489821

IntechOpen